Environ. Sci. Technol. **1998**, *32,* 2614−2622

Activated and Nonactivated Forms of Zinc Powder: Reactivity toward Chlorocarbons in Water and AFM Studies of Surface Morphologies

TATIANA N. BORONINA,[†] ISABELLE LAGADIC,[†] GLEB B. SERGEEV,[‡] AND KENNETH J. KLABUNDE*,[†]

Department of Chemistry, 111 Willard Hall, Kansas State University, Manhattan, Kansas 66506, and Department of Chemistry, Lomonosov Moscow State University, 119899 GSP Moscow, Russia

This work was carried out with the purpose of developing effective reagents for decontamination of groundwater contaminated with chlorocarbons. Zinc metal as a reducing agent for carbon tetrachloride (CT), chloroform (Chl), and methylene chloride (MC) in aqueous solution has been studied in some detail, especially regarding activated forms of the metal. Chlorocarbon concentrations were monitored at certain time intervals by gas chromatography/mass spectrometry (GC/MS) analysis of the headspace and water phase. Reaction mixture headspace was additionally studied by a GC/headspace analysis system to detect the formation of hydrocarbons. Chloroform, methylene chloride, methyl chloride, methane, and acetylene were found to be products from CT reduction. For methylene chloride reduction, traces of *cis* and *trans*-1,2-dichloroethene (DCE) were also found. Activated by cryo or mechanical treatment, metallic zinc caused an increase in CT dechlorination rate and conversion into methane. After the first 2.5 h, more than 20% of CT was converted into methane by cryochemically activated zinc in comparison to 1.2% by conventional zinc dust. Furthermore, CT reduction by activated zinc caused the formation of DCEs and TCE. Pathways are proposed to account for the observed methane/methylene chloride ratio and DCEs and TCE formation that include sequential reductive dechlorination through organometallic and carbonoid species on the Zn surface. Furthermore, it seems likely that some methane can be formed in "one metal contact", since significant amounts are formed early in the reaction. In attempts to learn more about morphological changes in the zinc during its consumption, pore volume/pore radii were determined, and atomic force microscope images were obtained. Zinc corrosion takes place rapidly at edges/corners leading to the formation of cavities with wide openings, large volumes, and increased specific surface areas. Pyramidal zinc "pillars" are formed during the process.

* Corresponding author fax: (785)532-6666; e-mail: KENJK@KSU.EDU.

[†] Kansas State University.

[‡] Lomonosov Moscow State University.

Introduction

The widespread use of chlorinated solvents in commerce has led to considerable groundwater contamination. Most chlorocarbons have been found to have long half-lives in the natural subsurface environment (*1*). Chloroalkanes, including chloroform and carbon tetrachloride, have a cumulative toxicity and are carcinogenic. Sweeny (*2*, *3*) followed by Senzaki and Kumagai (*4*, *5*) were the first to report an environmental application of zero-valent iron for removal of chlorinated compounds from water, and they formulated some preliminary ideas for aboveground treatment reactors. Further interest in the use of zero-valent metals can be attributed to Gillham and O'Hannesin (*6*, *7*), who proposed the use of permeable walls containing metallic iron as a reactant, and Reynolds with co-workers (*8*), who reported on aliphatic halide transformation in the presence of several metals, including iron, galvanized metals, aluminum, and copper. Clearly, the use of zero-valent metals has been an active research area (*9*−*27*) with efforts mostly concentrated on iron-containing water systems due to the success encountered with iron-loaded subsurface permeable walls (*27*) and the acceptance of zero-valent iron as being safe for the environment.

For the optimal design of remediation systems, precise information about reaction pathways and products formed is essential. Furthermore, complete dechlorination of the chlorocarbons is necessary since partial dechlorination does not remove the toxic threat and can even make the situation worse. Hence, the reduction of trichloroethylene (TCE) and perchloroethylene (PCE) by metallic iron in water has been thoroughly examined (*5*−*7*, *12*, *13*, *19*−*26*) with attention given to reaction mechanism, kinetics, and volatile products—hydrocarbons and volatile chlorocarbons and carbon mass balance account.

Much less attention has been given to metals other than iron, although it is known that galvanized metals react quite rapidly with chlorocarbons (*8*). In fact, metallic zinc was reported to cause deep (more complete) sequential dechlorination of carbon tetrachloride with methane being one of the final products (*17*, *18*). Furthermore, TCE and PCE have been found to undergo deep dechlorination by zinc (*22*, *28*, *29*).

Chlorocarbon dechlorination in water by zero-valent metals is considered to be a heterogeneous process in which the observed reaction rate depends on surface area (*7*, *21*). On the basis of detailed analysis of CT and TCE reduction on *iron*, it was concluded that direct electron transfers are important in determining the rate (*9*, *20*). Furthermore, it has been proposed that only one surface contact of CT with a *zinc* surface can cause complete reduction to CH_4 (*30*, *31*).

Since this chemistry is largely controlled by liquid−solid interactions, it should not be surprising that the physical state of the metal is important. High surface areas and reactive surface sites should be crucial, and this means that ways of activating the metals should be important. There are many ways to do this (*32*). Mechanical means (striking, splitting, grinding) are common methods, although usually only micron-size particles can be obtained (*33*, *34*). A more effective way is by metal vapor (atom) agglomeration in low temperature solvents (solvated metal atom dispersion (SMAD) also called cryochemical activation due to the low temperatures employed) (*34*−*36*). Nanometer-sized crystals with non-oxidized surfaces possessing many reactive edge/corner sites are obtained by this method. Removal of solvent leaves a very reactive nanoscale metal powder. This method is wide

S0013-936X(97)00997-8 CCC: $15.00
Published on Web 07/17/1998

in scope such that a variety of solvents and almost any metal can be employed (*35*−*38*). Although these methods of activating metals are expensive and perhaps do not lend themselves to practical application, studies of their reactivity toward toxic materials in aqueous systems show what is possible to achieve and lend greater understanding of this complex chemistry.

In this study, the dechlorination of CT is examined in a batch metallic zinc−water reactor system. Along with commercial zinc, mechanically and cryochemically activated forms of zinc were used in an attempt to increase the reaction rate and CT conversion into completely reduced gaseous products, such as methane. To acquire information about surface topology, area, and pore size distribution, zinc surfaces were studied by atomic force spectroscopy (AFM) and multi-BET/BJH gas adsorption methods.

Experimental Section

Zinc Particles Employed toward Chlorocarbons in Water. Three kinds of zinc particles were employed for chlorocarbon dechlorination; Zn(0) dust, zinc cryoparticles, and mechanically activated zinc dust.

Commercial Zn(0) dust (Fisher, certified grade) was used without further cleaning or treatment. Nitrogen BET adsorption analysis indicated a specific surface area of 0.25 m^2/g.

Zn cryoparticles were prepared by means of low-temperature technique, described in detail elsewhere (*35*−*38*), and involved co-deposition of metal and organic solvent (pentane or toluene) vapors on the reactor walls at 77 K, followed by warming to room temperature and solvent evaporation. Surface area and reactivity of the cryoparticles prepared by this method depend on experimental conditions—the speed of solvent and metal evaporation, solvent/metal ratio, etc. Depending on the metal employed, surface areas as high as 100 m^2/g can be achieved. In the present study, 5 g of Zn was co-deposited with 200 mL of solvent leading to surface areas of about 5.5 m^2/g. Cryoparticle samples were handled and stored under argon in a dry cabinet.

Mechanically activated zinc was prepared by pressing commercial Zn dust at ambient conditions at 2000 psi into pellets of 5 mm in diameter and mass of 0.025 ± 0.003 g or at 7000 psi into pellets of 13 mm and of $0.60 + 0.01$ g. Five 5-mm pellets of total mass 0.11 g or one 13-mm pellet was added to each vial and employed toward carbon tetrachloride. Nitrogen multi-BET analysis indicated a specific surface area of 3.2 m^2/g for five 5-mm pellets. (This type of pressure-induced activation, causing higher surface areas and enhanced reactivity, is due to crushing and cleavage of larger Zn particles thus yielding higher proportions of clean Zn surface.)

Zn Particle and Solid Products Characterization. Specific surface area and pore size distribution determinations were done by employing a NOVA Quantachrome instrument using nitrogen Mullet−BET analysis and the BJH method. The density of zinc dust determined on the NOVA Quantachrome was 7.0 g/cm^3. That is close to 7.14 g/cm^3 for zinc metal (*39*). Nitrogen single-point BET analysis was done for a number of samples on a Micrometrics flowsorb II 2300 instrument.

Carbon and hydrogen elemental analysis was performed for zinc dust and cryoparticles by Desert Analytics (Tucson, AZ).

Powder X-ray Diffraction (XRD) analysis and thermogravimetric analysis (TGA) were used to identify solid products. To collect the zinc−products mixture, the reaction solution was decanted, the remaining solid was dried at room temperature under argon, and stored under argon before analysis.

X-ray diffraction patterns were recorded on a Scintag-XDS-2000 instrument. The spectrometer was set at a voltage of 40 kV, and current was 40 mA. The scans were taken from 20 to 85° 2Θ at a scanning rate of 2° 2θ/min.

TG analysis was carried out on a Shimadzu TGA-50, and the zinc product mixtures (0.02 g) were heated from 22 to 600 °C at 10 °C/min.

Atomic force microscopy (AFM) study was performed to observe the surface topology of zinc pellets of 5 and 13 mm in diameter (mechanically activated zinc) and the change occurring upon the reaction with carbon tetrachloride. Preliminary studies had been carried out to determine how the applied pressures of 2000, 3000, 5000, and 7000 psi affected the surface topology of a pellet of 5 or 13 mm in diameter and to choose the optimum pressure ratio giving a reproducible surface morphology. Imaging the pellet surface was carried out on the commercial AFM (SPM 30 from Wyko Inc.) in the contact mode. A 100 μm long and rectangular cantilever with a spring constant of 0.37 N/m and a Si_3N_4 integrated pyramidal tip were employed. All images were obtained at ambient conditions.

The AFM experiments were performed on different parts of each surface and at least twice at the same point to ensure that the observed surface morphology was reproducible and representative. The strategy of "sequential magnification" was applied to study the morphology of each particular point on the surface. First, the image was obtained with a scan range of 50 or 20 μm. Then, the features of interest were examined at higher magnification using a succession of 5.0 and 3.0 or 2.0 and 1.0 μm scan ranges. The same pellet was studied before and after reaction, and data acquired on all pellets were consistent with respect to pressures and reaction times.

Dechlorination of Chlorocarbons by Zn. Dechlorination experiments were performed in closed batch systems. To study the kinetics of CCl_4 dechlorination by Zn, experiments were conducted in 40-mL glass amber vials capped with Teflon Mininert valves. Each vial contained zinc (0.1, 0.5, or 2.0 g of dust; 0.11 g of pellets; 0.1 or 0.5 g of cryozinc) suspended in 28 mL of deoxygenated water−CCl_4 solution. Thus, 12 mL of headspace was initially present. Overall, the CCl_4 concentration ranged from 0.9 to 1.1 mM (based on water volume). The procedure for reaction mixture preparation was as follows: 28 mL of distilled water in each 40-mL vial was sparged with purified argon for about 25 min, and the vials were capped with Mininert valves (screw cap). Three microliters of neat CCl_4 was injected through the valve beneath the water level. Vials were intensively mixed overnight lying on their sides on a homemade rocker. To ensure that CCl_4 was completely dissolved and to determine its exact initial concentration, the water phase was analyzed by GC/MS. Before the sampling, vials were kept upright for 15 min on a low speed rotomix (Fisher) rotator at 60 rpm to attain the CCl_4 concentration equilibrium between the gaseous and liquid phases.

After the initial concentration had been determined, vials were cooled to about 10 °C for 10 min to diminish the amount of volatiles in the headspace, zinc particles were added to the solution, and vials were immediately capped and placed on the shaker lying sideways. Zinc cryo, 0.1 or 0.5 g, was weighed in an argon atmosphere and added to the reaction solution immediately after weighing. Mixing was done on the rotator at 60 rpm. In blank experiments (no metal added), all the CCl_4 was detected with good precision (±5%). A number of experiments were carried out using the above procedure to study dechlorination of chloroform and methylene chloride in water by zinc dust (2.2 g). where the initial chlorocarbon concentration in water was about 0.5 mM.

Gas Chromatography/Mass Spectrometry (GC/MS) and GC Analyses. The change in chlorocarbons and methane concentration during the course of the reaction was followed by periodic sampling from a single vial. During the 15 min before sampling, each vial was kept upright on the mixer to allow an equilibrium chlorocarbon concentration between two phases to be attained. Each vial was sampled twice with a difference in time of 1.5−2.0 min. To identify chlorocarbons and to determine their concentrations, one aliquot was analyzed by GC/MS with direct water (0.6 μL) or headspace (100 μL) injections. To follow methane formation, another aliquot of reaction headspace (200 μL) was analyzed by GC. A water aliquot was taken using a 10-μL gastight syringe (Hamilton), and headspace was taken by using a gastight 2-mL syringe equipped with a Teflon Mininert valve.

The GC/MS analysis was carried out on the Perkin-Elmer auto system gas chromatograph/Q-Mass 910 mass spectrometer using selected ion monitoring (SIM) scan acquisition and 30 m × 0.25 mm, 1.4 μm crossbond 5% phenyl−95% methyl polysiloxane capillary column (Restek Rtx-502.2). Direct water or headspace injections were performed using the following conditions: helium pressure 45 psi, the injector port temperature 240 °C, detector 220 °C, the AUX zone temperature 230 °C, the column temperature program 33° (1 min)—at 2 °C/min to 45 °C/min to 240 °C (3 min). Additional GC analysis was performed on the series 580 GOW-MAC isothermal gas chromatograph with a TCD detector and helium as carrier gas. Methane concentration was determined using a Carbosphere 60/80 mesh, 6 ft, 1/8 in. SS packed column (Alltech) at a helium flow of 40 mL/min, column temperature of 140 °C, injector temperature of 220 °C, detector temperature and current of 160 °C and 200 mA, respectively. The formation of acetylene was detected in the same column at a column temperature of 180 °C, detector temperatures of 200 °C, and detector current of 180 mA.

A number of blank experiments (no zinc) were carried out to obtain a set of calibration curves in GC/MS (or GC) peak area versus chlorocarbon (methane) concentration plots for water phase and headspace.

Hydrocarbon Identification during Carbon Tetrachloride Dechlorination by Zinc Dust and Cryozinc. A number of experiments on carbon tetrachloride dechlorination were performed in 22-mL vials for the headspace analysis. Vials contained 5 mL of distilled deoxygenated (Ar-sparged) water to which 0.5 g of zinc dust or cryozinc was added, and 0.5 mL of saturated CCl_4 stock solution was injected beneath the water level. Vials were immediately crimped, shaken, and put into the carousel of the headspace analyzer being kept at 32 °C. A Varian Stat 3600 CX GC−genesis headspace analyzer system was equipped with a FID detector and GasPro GSC 30 m × 0.32 mm capillary column (Alltech). This combination of equipment with a PLOT capillary column made it possible to analyze hydrocarbons and volatile chlorocarbons in one run. The sampling loop and transfer line of the headspace analyzer were kept at 200 and 210 °C, respectively. The transfer line ended with a needle that was introduced through the septum into the injector port at 210 °C. Helium flow was 3.5 mL/min, detector temperature was 300 °C, column temperature program was 36 °C (3 min) at 10 °C/min to 60 °C and at 15 °C/min to 180 °C at 25 °C/min to 240 °C (2 min). The high ratio of headspace to solution volume in these experiments provided an advantage for volatile reaction products and intermediates, especially hydrocarbons, to partition into the headspace rather than remaining in solution or sorbing to the metal surface (*1*) and facilitated their detection. Hydrocarbon detection for iron systems in the absence of chlorocarbon have been reported (*4*, *24*, *26*); therefore, we carried out blank experiments with no carbon tetrachloride added for both dust and cryozinc particles to ensure that hydrocarbons detected were only due to the reaction of Zn with carbon tetrachloride.

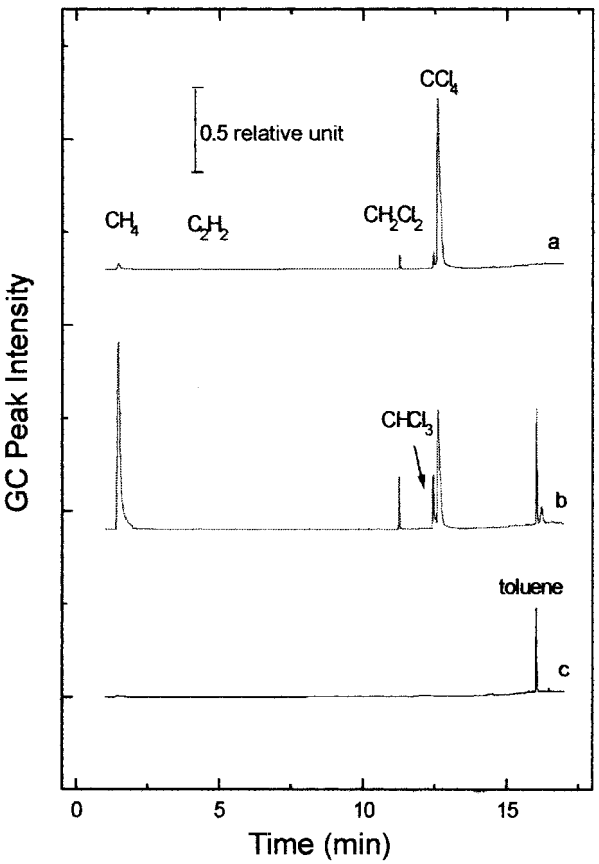

FIGURE 1. Chromatograms of the reaction headspace after 2.25 h of carbon tetrachloride dechlorination by different types of zinc metal samples in water (5 mL of 0.5 mM CT water solution in 22 mL vial for headspace analysis and zinc 0.5 g) (a) zinc dust, (b) cryozinc, (c) blank, cryozinc in water. Toluene peak in panels b and c is due to cryoparticle method of preparation.

pH and Cl^- Ion Concentration Measurements. The measurements were carried out on an Orion pH/mV meter model 290A using an Orion combination pH electrode and Cl^- ion selective electrode. Two point calibration of the pH electrode was performed daily using 2.0 and 7.0 standard buffer solutions (Fisher). The ion selective electrode was calibrated every 2 h using a set of standard solutions. The pH and Cl^- ion concentration before reaction were measured in blank experiments, after reaction-in filtered solutions. No pH buffer was employed.

Results and Discussion

Kinetics of Chlorocarbon Dechlorination in Water by Zinc Metal Particles. Products observed for chlorocarbon dechlorination by zinc and activated zinc particles are shown in Figures 1−3 and Tables 1 and 2. Earlier we reported in refs *17* and *18* that zinc dust caused carbon tetrachloride sequential degradation through intermediate chloroform and methylene chloride into methyl chloride, methane, zinc chloride, and zinc hydroxide. Acetylene was also found to be a product (*30*, *31*). For reaction times of 480 h, *cis*- and *trans*-1,2-dichloroethylene (DCE) in concentrations of 0.001−0.003 mM were detected (Tables 1 and 2). Zinc hydroxide formation was confirmed by powder XRD and are confirmed by TGA in the present study (*17*, *18*). Thus, TGA data indicated two peaks at 120 and 250 °C on the weight loss versus temperature curve. The first one was assigned to zinc hydroxide (decomposes at $T > 121$ °C; *39*). Weight loss at

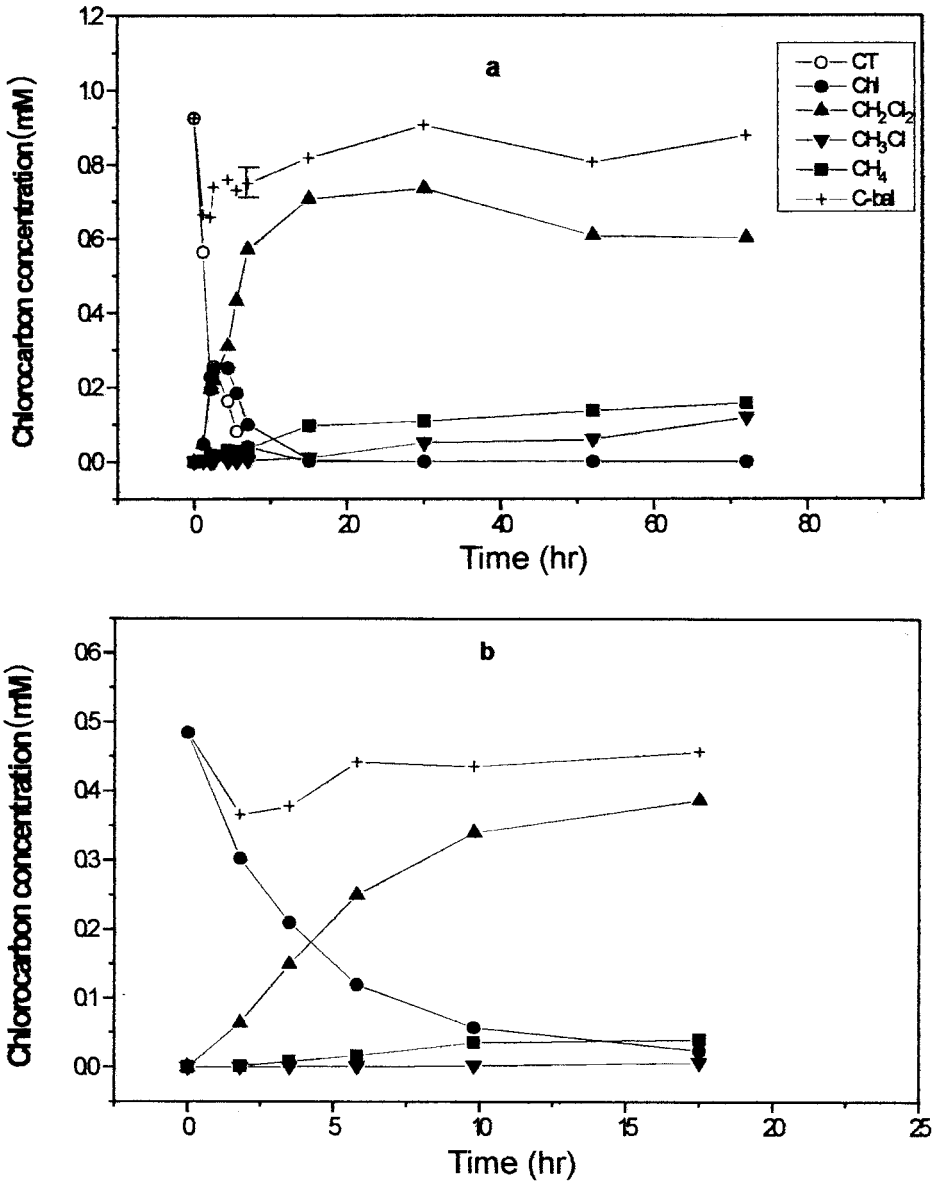

FIGURE 2. Chlorocarbon dechlorination in water by zinc dust 2.2 g, surface area concentration (SAC) 10.1 m^2/L in 40-mL vials with 28 mL of water/12 mL of headspace. Carbon balance without acetylene. (a) Carbon tetrachloride 0.925 mM. (b) Chloroform 0.485 mM.

250 °C was about 0.2−0.3% for all samples analyzed, it did not change with reaction time, and its cause has not been identified.

Chloroform was easily dechlorinated in water by zinc dust with the same major products (Table 1, Figure 2b). Again, as for carbon tetrachloride, conversion into methane was higher than into methyl chloride at the earlier reaction times. After approximately 140 h (Tables 1 and 2), the situation has inverted and also 0.001−0.003 mM of *trans*- and *cis*-DCE was detected.

Pure methylene chloride was also found to degrade in the presence of zinc dust, though much slower. *trans*- and *cis*-DCE were determined to be products (Tables 2 and 3), and methylene chloride conversion into methane was slow as compared with methyl chloride formation. Thus, in the course of CT and Chl degradation, we believe that much of the methyl chloride and DCE originate from degradation due to a pathway where CH_2Cl_2 is an intermediate.

Use of mechanically and cryochemically activated particles affects carbon tetrachloride degradation in water in quite similar ways. For both kinds of activated zinc particles, major products are the same as for dust, but DCEs and also TCE formation was observed at earlier reaction times and in higher concentrations (Tables 1 and 3). Also, the solutions became more acidic in comparison with zinc dust (Table 3). It is most important that both mechanically and, especially, cryochemically activated particles *enhanced the percent of carbon tetrachloride converted into methane* (Table 3 gives rates of CCl_4 degradation for each type of metal sample.) Interestingly, zinc pellets exhibited lower first-order rate constants for carbon tetrachloride degradation (k_{obs}), whereas cryoparticles caused both an increase in methane production and k_{obs} (Figures 1 and 3; Table 3). Element analysis has indicated a larger carbon and hydrogen content in cryoparticles as compared to dust: 1.15−1.40 and 0.10−0.13% versus 0.07 and 0.02%, that is, we assume, due to the method of synthesis. However, blank experiments with no carbon tetrachloride have shown that this carbon and hydrogen do not contribute noticeably to the amount of methane detected (Figure 1c).

pH Measurements. A pH buffer was not employed in these studies. Nevertheless, the pH remained relatively stable during carbon tetrachloride degradation, diminishing at most from pH 6.10−6.15 to pH 5.66−5.87 for zinc cryo and pellets

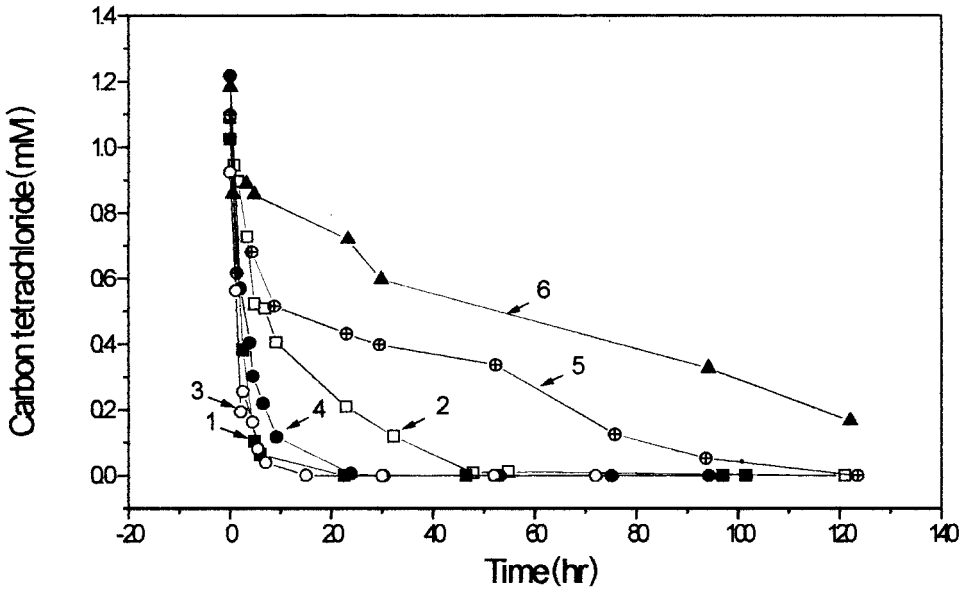

FIGURE 3. Carbon tetrachloride degradation by zinc metal particles in water. The 40-mL vials with 28 mL of water/12 mL of headspace; 0.925−1.2 mM CT. (1) Cryo 0.5 g, SAC 93.4 m^2/L; (2) cryo 0.1 g, SAC 18.7 m^2/L; (3) dust 2.2 g, SAC 19.1 m^2/L; (4) dust 0.5 g, SAC 4.33 m^2/L; (5) dust 0.1 g, SAC 0.87 m^2/L; (6) pellets 0.11 g SAC 13.1 m^2/L.

TABLE 1. Products Observed upon Chlorocarbon Dechlorination in Water by Zinc Dust and Activated Zinc Particles for Reaction Times up to 480 h

reaction	products observed
Zn(s) dust + CCl_4(sol)	intermediate $CHCl_3$(sol), CH_2Cl_2(sol); CH_3Cl(g), CH_4(g), C_2H_2(g), H_2(g), plus traces of *trans*-/*cis*-DCE(sol) (long term reaction, refer to Table 2), $ZnCl_2$(sol); $Zn(OH)_2$(s), traces of ZnO(s)
Zn(s) cryo + CCl_4(sol)	the same ($CH_3Cl \ll CH_4$) + TCE(sol), *trans*-/*cis*-DCE(sol)
Zn(s) pellets (mechanically activated) + CCl_4(sol)	the same as for cryozinc
Zn(s) dust + $CHCl_3$(sol)	intermediate CH_2Cl_2(sol); CH_3Cl(g), CH_4(g), H_2(g) plus traces of *trans*-/*cis*-DCE(sol) (long-term reaction, refer to Table 2), $ZnCl_2$(sol)[a]
Zn(s) dust + CH_2Cl_2(sol)	CH_3Cl(g) (vinyl chloride?) > CH_4(g), H_2(g), *trans*-/*cis*-DCE(sol), $ZnCl_2$(sol)[a]

[a] Acetylene and solid products were not analyzed; traces of Zn $(OH)_2$ were determined by XRD (*17*).

TABLE 2. Chlorocarbon Dechlorination in Water by Zinc Dust[a]

chlorocarbon and its initial concn (mM)	reaction time (h)	k'_{obs}[b] (h^{-1})	conv. into CH_4 (%)	conv. into CH_3Cl (%)	conv. into DCEs (%)	carbon bal[c] (%)	pH	Cl bal (%)
CT 0.925	5.5	0.538 ± 0.081	3.1	0.2		79 ± 4	6.01	n/d
0.925	52.0		14.8	6.6		87 ± 4	7.17	n/d
0.925	72.0		17.1	12.9		95 ± 4	n/d	81.3
0.925	480.0		27.5	37.9	~0.3	93 ± 4	6.79	89.2
Chl 0.485	5.8	0.241 ± 0.021	3.4	0.21		101 ± 5	6.50	96.5
0.485	140.0		31.5	21.4	~0.5	96 ± 4	n/d	n/d
CH_2Cl_2 0.446	52	0.0037 ± 0.0005	6.4	5.16	3.8	96 ± 4	7.17	95.1

[a] 2.2 g of zinc dust in 40-mL vials containing 28 mL of water/12 mL of headspace; surface area concentration, 19.1 m^2/L. [b] Observed first-order rate constant of chlorocarbon degradation determined over the first 6 h for CT and Chl; 52 h for CH_2Cl_2. [c] Carbon balance without acetylene.

and staying almost unchanged at pH 6.04−6.17 for dust (Tables 2 and 3). The pH versus time dependence for the reaction of zinc dust with carbon tetrachloride was described earlier, and it was shown that the dependence exhibited a small maximum over the first 1−2 h. Its position seemed to depend on experimental conditions, such as reactant concentration, the method of mixing, etc., that might affect the competition between metal reaction with carbon tetrachloride and with water. We assume that zinc oxidation by water yielding zinc hydroxide and hydrogen causes the increase in the pH, and carbon tetrachloride reductive dechlorination by zinc leads to zinc chloride that makes the pH more acidic, working to some extent as a buffer. The pH appeared to be slightly more basic for chloroform and methylene chloride degradation by zinc dust (Table 2).

BET and Pore Size Distribution Analyses of Zinc Particles during Reaction with CCl_4. Since specific surface areas of metal samples actually increased during reactions with CCl_4−H_2O, it seemed important to better understand the morphological changes taking place. Results obtained by multi-

TABLE 3. Characteristics of Carbon Tetrachloride Degradation in Water by Different Kinds of Zinc Particles[a]

zinc type and mass (g)	spec. surface area before/120 h (m^2/g)	surfce area concn (m^2/L)	k'_{obs}[b] (h^{-1})	k_1[c] (h^{-1} L m^{-2})	conv. into CH_4, 120 h (%)	carbon bal[d] 2/120 h, (%)	pH, 120 h
cryo 0.5	5.23 ± 0.25/8.54	93.3	0.473 ± 0.025	0.0051 ± 0.0003	36.4	70.2/50.0	5.87
cryo 0.1	5.23 ± 0.25/not det.	18.7	0.084 ± 0.006	0.0045 ± 0.0003	27.3	82.0/52.1	5.66
dust 2.2	0.243/1.4	19.1	0.538 ± 0.081	0.0282 ± 0.004	17.1 (72 h)	71.2/94.7 (72 h)	not det.
dust 0.5	0.243/1.4	4.33	0.208 ± 0.009	0.048 ± 0.002	25.9	83.5/99.5	6.17
dust 0.1	0.243/not det.	0.87	0.026 ± 0.003	0.030 ± 0.003	14.5	85.2/92.6	6.04
pel. 0.11	(3.34/2.52)[e]	13.1	0.0144 ± 0.0004		31.3	81.5/93.6	5.79

[a] 40-mL vials with 28 mL of water/12 mL of headspace; initial CT concentration, 0.925 mM with 2.2 g of zinc dust and 1.1−1.2 mM in other reactions. [b] k'_{obs}, observed first-order rate constant of CT degradation in water. [c] $k_1 = (k'_{obs}$/initial surface area concn), specific rate constant of CT degradation. [d] Without acetylene, DCEs and TCE. [e] Determined values are shown, but they may not be reliable since, in this case, the desorption isotherm was below the absorption isotherm.

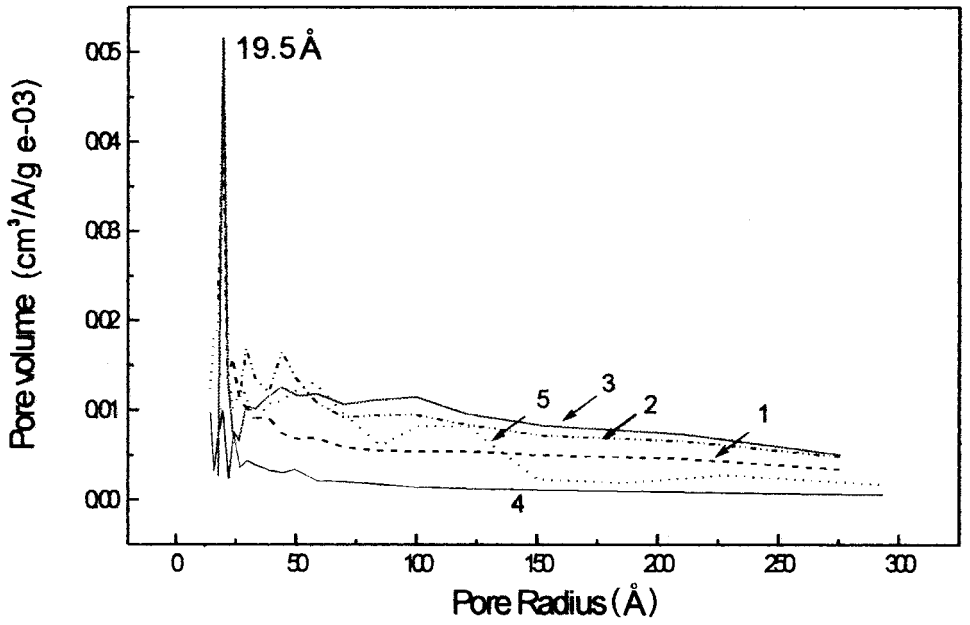

FIGURE 4. Zinc dust pore volume distribution change upon carbon tetrachloride (0.925 mM) dechlorination in water in (1) 5.8, (2) 15.0, and (3) 52.0 h and zinc dust (4) before reaction and (5) in 96 h in water without CT.

BET and BJH methods are shown in Figures 4 and 5. Zinc dust exhibited only noise at 19−29 Å in the total pore volume versus pore radius plot. Upon reaction with carbon tetrachloride or pure water, both the specific surface area and total pore volume increased in such a manner that they attained a maximum. The average pore radius value exhibited an increase initially during the reaction and then a decrease. In the reaction with CT, the total pore volume in the whole radius range was enhanced over time (Figure 4). A number of maxima appeared at similar radii values below 150 Å in the total pore volume versus pore radius plot. Note the large peak at 19.5 Å that developed for the $Zn-H_2O$ reaction (no CT) and the long reaction time with CCl_4-H_2O.

Zn cryo particles before reaction had 20 times larger specific surface area and 40 times larger total pore volume, but a smaller average pore radius as compared to dust (Figure 4 vs Figure 5). In 120 h of reaction with CCl_4, the specific surface area and pore volume (radius) was enhanced. The peak at 19.5 Å, which was significant even before reaction, increased by a factor of 10 in height during this time.

There are at least two factors affecting the metal-reactant pore volume distribution and average radius upon chemical reaction—an erosion of surface due to the metal consumption and solid products precipitation. Each of them, depending on intrinsic details of metal consumption and solid precipitate characteristics, could diminish or enhance the surface pore radius and volume. Results suggest that the CT−Zn reaction causes pore radius/volume increase over the whole radius range, whereas oxidation by water leads mostly to the formation of narrow pores. The featured peak at 19.5 Å could be attributed to water erosion of metal or to products (zinc oxide/hydroxide). Indeed, it could be assigned to zinc oxide for the following reasons: (a) $Zn(OH)_2$ product would be dehydrated to ZnO during the required preheating step (180 °C) prior to BET analysis. (b) It is known that such dehydration procedures can lead to bottleneck pores. Thus, we tentatively conclude that corrosion by water leads to narrow pores indirectly by ZnO formation, which itself then generates such pores. On the other hand, corrosion by $CT-H_2O$ leads to rapid consumption of zinc at reactive sites (corners, edges), leading to the formation of cavities possessing large openings and large volumes.

AFM Study of Zinc Pellets and Cryoparticles. AMF images of Zn pellets are presented in Figure 6. Pellets of 5 mm in diameter, 0.025 g in weight made at 2000 psi and those of 13 mm and 0.7 g pressed at 7000 psi exhibit quite similar uniform, reproducible features (Table 4). To obtain the similar surface morphology for pellets of different diameter, we varied mass and pressure, keeping unchanged the ratio

$$(\text{applied pressure} \times (\pi/4)\ \text{diameter}^2/\text{mass})$$

This ratio determines the morphology details that could be seen (how "smashed" a surface is) and is about 500 psi × $mm^2 \times g^{-1}$ for the two appropriate sets of parameters. A

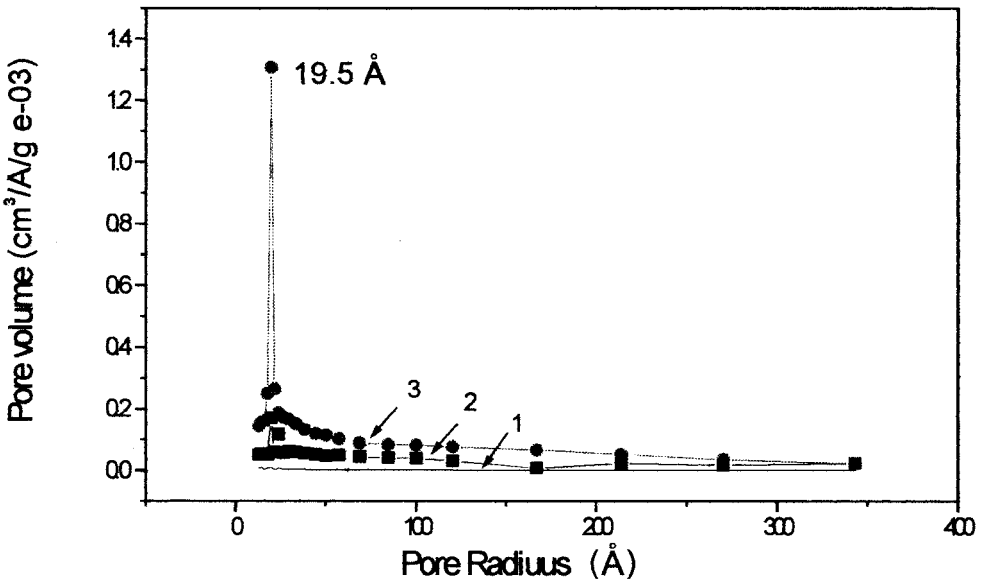

FIGURE 5. Pore volume distribution change for zinc cryoparticles after reaction with carbon tetrachloride in water, 40-mL vials with 28 mL of water/12 mL of headspace; 0.5 g of cryozinc and 1.2 mM CT. (1) Zinc dust before reaction, SSA 0.243 m^2/g; zinc cryo (2) before reaction, SSA 5.23 m^2/g and (3) after 120 h reaction, SSA 8.54 m^2/g.

TABLE 4. AFM Study of Zn Dust Pressed at Different Pressures into Pellets of 5 mm in Diameter and 0.020−0.025 g in Mass

pressure (psi)	20-mm scan	5-mm scan
2000[a]	Macro units, topless cones 800−1200 nm in height and 200−1000 nm in diameter (average about 500 nm)	slightly elongated particles 100−300 nm in length on a unit top
3000	unit tops are smashed and look more like cylinders, average diameter 700−1000 nm	almost the same as at 2000 psi
5000	morphology is not uniform in the pellet center and edges; center, no individual units (or no space between units)	elongated particle 300−400 nm, look as if they are separated from each other
	closer to the edge it becomes possible to see the contour of units and near the edge; to distinguish individual units	elongated 200−300, similar to ones at 2000 psi

[a] The same topology was observed for zinc dust pressed at 7000 psi into pellets of 13 mm in diameter and 0.6 g in mass.

pellet surface before reaction is quite well-organized in units of similar shape, topless cones, and almost cylinders (Figure 6a). Unit height is about 1000 nm, and diameter at the top ranges from 200 to 800 nm. In 3D, each unit appeared to be a stack of topless triangles, staying upright or slightly tilted. Thus, these units form a kind of surface macrostructure, and then particles of 100−300 nm on the unit top could be considered as a microstructure. A surface plot for zinc dust metal (not shown) does not exhibit these features.

Upon reaction with carbon tetrachloride the surface topology changes sequentially (Figure 6). During the first 1−2 h the enlargement of the particles in the unit top becomes noticeable, but the macrostructure remains almost untouched. Further erosion affects the macrostructure, and in 25 h some of the units are "eaten off" and others transform into triangular stacks of 8−10 μm in base and about 2.0−2.5 μm in height. The particle size of the microstructure increases to 300−400 nm (Figure 6b,c). In the blank experiment (Figure 6b), particles enlarge more (400−500 nm), but at the same time it is possible to see that their surface was further eroded and consisted of 50−100 nm particles. After 48 h reaction with CT there are only traces of the initial unit left. It seems that they were replaced by large triangular stacks (Figure 6c). Those stacks might represent some structure (for example, the units that were initially tilted) that for some reason was touched by erosion to a lesser degree. They may be attributed to the hexagonal zinc structure because very similar features were observed for zinc cryoparticles (Figure 6d). On a 5-μm scan, the surface of zinccryo looks planar and displays units isolated from each other. The "plane surface" observed for pellets after 25 h and especially 48 h of reaction is most likely formed as a result of surface erosion plus product precipitation. For Zn cryo, this type of surface exists even before the reaction with CT, which probably indicates that highly reactive cryoparticles were oxidized with air. That is consistent with assignment of the 19.5 Å peak in the pore volume versus pore radius plot (refer to Figures 4 and 5) to zinc oxide. The air-sensitive plane surface makes it difficult to scan, especially 1−2 μm ranges, and poor quality pictures were obtained. For cryozinc after reaction with CT, we were not able to obtain any images.

Conclusions and Implications

Carbon tetrachloride dechlorination occurs in the presence of all three zinc metal forms in aqueous systems. Mechanically and cryochemically activated zinc enhanced methane formation from CT. Chlorocarbon degradation obeys the first-order kinetic equation, and the observed first-order kinetic constant k^1_{obs} was used to compare reactivity of metal particles (Tables 2 and 3). Cryozinc exhibited the highest reactivity, though less than might be expected regarding its large surface area; for example, for iron where there is a strong surface area-reactivity dependence (*11*). Carbon mass balance obtained for zinc dust ranged from 60 to 70% in the beginning of the reaction and about 90−95% at the end. Low carbon balance recoveries may for the activated forms of zinc be due in part to stripping of volatile constituents caused by H_2 evolution from the reaction of activated zinc with water.

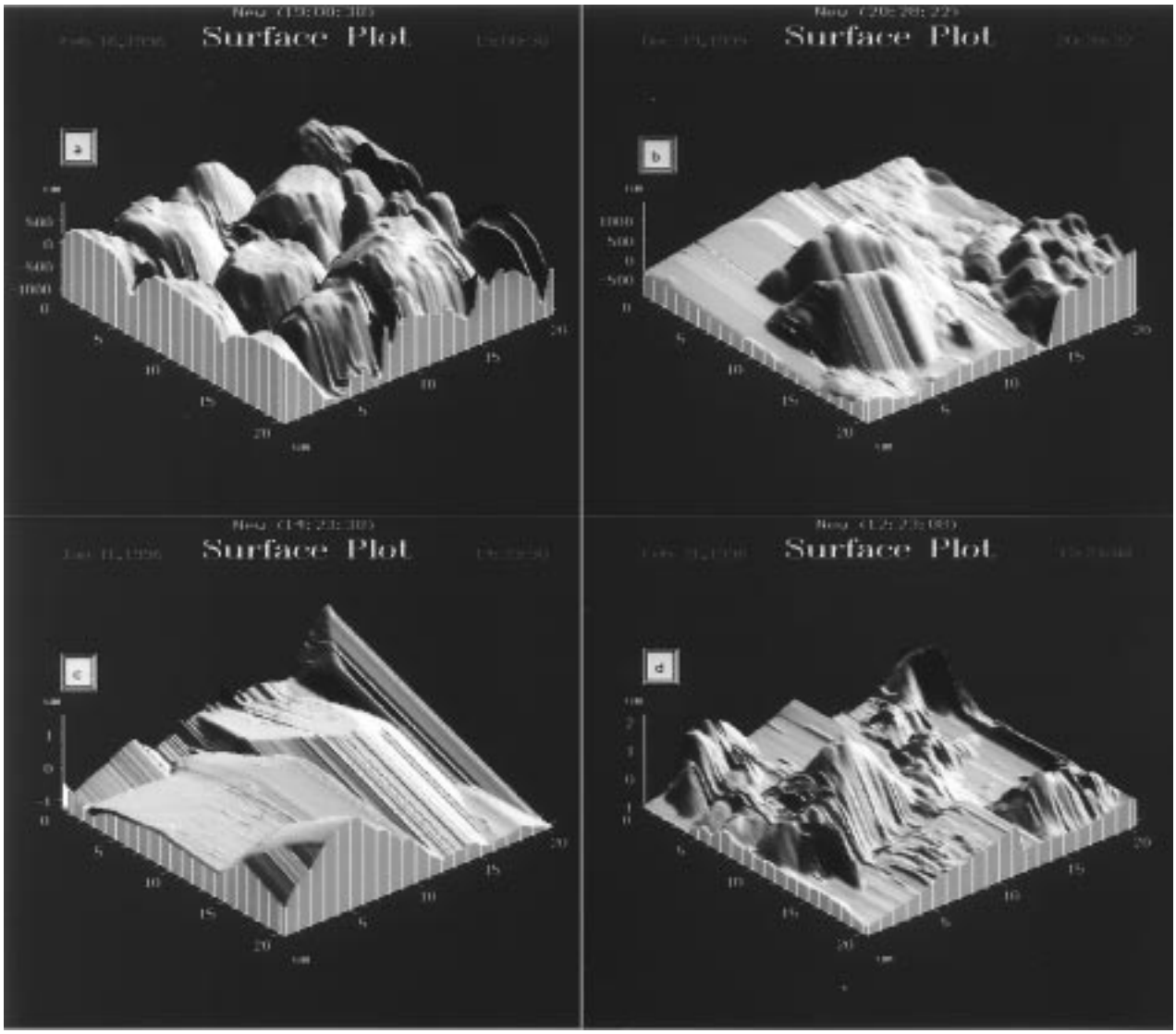

FIGURE 6. Atomic force micrographs of zinc dust pressed into pellets of 0.025 g and 5 mm in diameter at 2000 psi (a) before reaction, (b) after 24 h, and (c) after 48 h of reaction with 0.925 mM CCl_4 in water and (d) of zinc cryochips. Ambient conditions, 20 μm scan.

Kinetic curves in Figure 2 indicate that chloroform and methylene chloride are intermediate products in carbon tetrachloride degradation; likewise, methylene chloride is an intermediate in chloroform degradation. These findings reinforce the idea that a sequential reduction process takes place, and this probably occurs by the steps shown in Scheme 1. However, the fact that at early reaction times methane evolution is higher than methyl chloride (Table 2), coupled with the fact that acetylene, DCE, and TCE are also formed (Table 1), indicate that other reaction pathways are also possible. Furthermore, for carbon tetrachloride and chloroform dechlorination, the persistent drop in carbon balance observed over the first 2−5 h (Figure 2) of reaction could be regarded as due to chlorocarbon adsorption/chemisorption on the metal surface, similar to TCE, PCE, and CEs reversibly sorbed on iron (*19*, *25*).

The fact that both DCEs and TCE were observed in the reaction with activated forms of zinc but only traces of DCEs were detected with dust, suggests that different pathways may be driven by different active sites. Dechlorination via intermediate organometallic compounds was suggested earlier (*17*, *31*), and we still consider it to be important because, as the latest results have shown, the metal surface could play a multiple role. For example, on a zinc surface with many active sites (edges, corners, defects, etc.), the CCl_4 molecule could be sequentially and multiply reduced so rapidly that CH_4 is formed before intermediate $CHCl_3$, CH_2Cl_2, or CH_3Cl can be desorbed. It is also possible that, during this process, carbenoid species may couple to form DCE or other alkenes:

$$HCl_2CZnCl \rightarrow HCCl_{(ads)} + ZnCl_2$$

$$2HCCl_{(ads)} \rightarrow \underset{\text{DCE}}{ClHC{=}CHCl}$$

Indeed, it is well-known that Zn serves as the best metal for carbenoid formation in the Simmons−Smith reagent, for example, for cyclopropanation of alkene by ICH_2ZnI (*40*). Furthermore, dichlorocarbene (CCl_2) is known to be relatively stable and is a common intermediate in organic synthesis of dichlorocyclopropanes (*41*).

Mechanically and cryochemically activated particles demonstrated that they have a lot in common in topology, reactivity, and products. Units of the pellet surface macrostructure—topless cone—look similar to those of cryozinc (Figure 6). Both kinds of activated particles substantially enhanced methane evolution as well as caused TCE/DCEs formation (Tables 1 and 3). Thus, gain in activity was accompanied with change in selectively.

SCHEME 1. Possible Steps in CCl_4 Reduction and TCE/DCE Formation with Activated Zinc

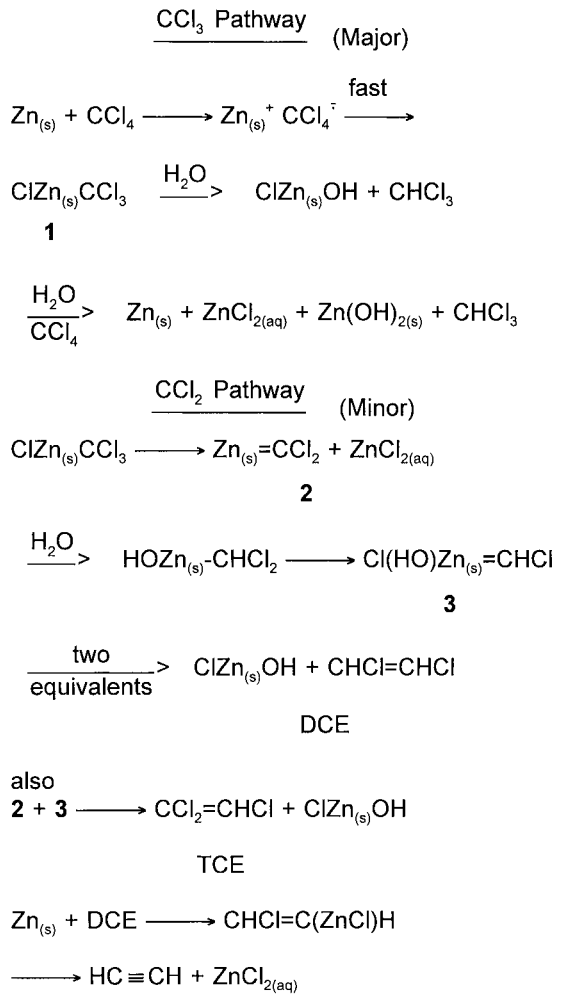

In summary, zinc metal (commercial dust, or cryochemically or mechanically activated) caused carbon tetrachloride dechlorination in water yielding methane, acetylene, methyl chloride, hydrogen, zinc hydroxide, and zinc chloride as major products. Near quantitative mass balance for the zinc dust studies indicate that all of the products have been found and identified. However, poorer mass balances were encountered with the active forms of Zn, which indicates that some carbon products or intermediates are adsorbed on the metal surfaces.

Sequential reductive dechlorination appears to be the major pathway, but on active metal surfaces these processes may occur partially by a one-metal-contact mode, yielding CH_4 at competitive rates with CH_3Cl, CH_2Cl_2, and $CHCl_3$.

The activated forms of zinc have similar morphologies before, during, and after extensive CCl_4 reaction. Erosion of the metal surface caused changes from columnar to pyramid-like structures, and surface areas, pore size, and pore volume increase as reaction with CCl_4 or H_2O proceeds. However, reaction with pure water yields small pore radii, while reaction with CCl_4 causes formation of larger pores with a broad pore radii distribution. These results are reasonably consistent with the competing pathways shown in Scheme 1.

Acknowledgments

The support of the Army Research Office and the Hazardous Substance Research Center at Kansas State University (funded by DOE and EPA) is acknowledged with gratitude.

Literature Cited

(1) Vogel, T. M.; Criddle, C. S.; McCarty, P. L. *Environ. Sci. Technol.* **1987**, *21*, 722−736.
(2) Sweeny, K. H. *Am. Water Works Assoc. Res. Found.* **1979**, *2*, 1487−1497.
(3) Sweeny, K. H. *Am. Inst. Chem. Eng. Symp. Ser.* **1981**, *77*, 72−78.
(4) Senzake, T.; Kumagai, Y. *Kogyo Yosui* **1988**, *357*, 2−7.
(5) Senzake, T.; Kumagai, Y. *Kogyo Yosui* **1989**, *369*, 19−25.
(6) Gillham, R. W.; O'Hannesin, S. F. *Ground Water* **1991**, *29*, 749.
(7) Gillham, R. W.; O'Hannesin, S. F. *Ground Water* **1994**, *32*, 958−967.
(8) Reynolds, G. W.; Hoff, J. T.; Gillham, R. W. *Environ. Sci. Technol.* **1990**, *24*, 135−142.
(9) Romanowski, W. *Highly Dispersed Metals*; PWN−Polish Science Publishers: Warsaw, 1987.
(10) Roush, W. *Science* **1995**, *269*, 473.
(11) Matheson, L. J.; Tratnyek, P. G. *Environ. Sci. Technol.* **1994**, *28*, 2045−2053.
(12) Schreier, C. G.; Reinhard, M. *Chemosphere* **1994**, *29*, 1743−1753.
(13) Lipczinska-Kochany, E.; Harms, S.; Millburn, R.; Sprah, G.; Nadarajah, N. *Chemosphere* **1994**, *29*, 1477−1489.
(14) Powell, R. M.; Puls, R. W.; Hightower, S. K.; Sabatini, D. A. *Environ. Sci. Technol.* **1995**, *29*, 1913−1922.
(15) Helland, B. R.; Alvarez, P. J. J.; Schnoor, J. L. *J. Hazard. Mater.* **1995**, *41*, 205−216.
(16) Warren, K. D.; Arnold, R. G.; Bishop, T. L.; Lindholm. L. C.; Beterton, E. A. *J. Hazard. Mater.* **1995**, *41*, 217−227.
(17) Boronina, T. N.; Klabunde, K. J.; Sergeev, G. C. *Environ. Sci. Technol.* **1995**, *29*, 1511−1517.
(18) Boronina, T. N.; Klabunde, K. J. *Natl. Meet. Am. Chem. Soc., Div. Environ. Chem.* **1995**, *35* (1), 759−762.
(19) Burris, D. R.; Campbell, T. J.; Manoranjan, V. S. *Environ. Sci. Technol.* **1995**, *29*, 2850−2855.
(20) Orth, W. S.; Gillham, R. W. *Environ. Sci. Technol.* **1996**, *30*, 66−71.
(21) Agrawal, A.; Tratnyek, P. *Environ. Sci. Technol.* **1996**, *30*, 153−160.
(22) Roberts, A. L.; Totten, L. A.; Arnold, W. A.; Boris, D. R.; Campbell, T. J. *Environ. Sci. Technol.* **1996**, *30*, 2654−2659.
(23) Hardy, L. I.; Gillham, R. W. *Environ. Sci. Technol.* **1996**, *30*, 57−65.
(24) Deng, B.; Campbell, T. J.; Burris, D. R. *Environ. Sci. Technol.* **1997**, *31*, 1185.
(25) Allen-King, R. M.; Halket, R. M.; Burris, D. R. *Environ. Toxicol. Chem.* **1997**, *16*, 424−429.
(26) Campbell, T. J.; Burris, D. R.; Roberts, A. L.; Wells, J. R. *Environ. Toxicol. Chem.* **1997**, *16*, 625−630.
(27) Gillham, R. W. *Natl. Meet. Am. Chem. Soc., Div. Environ. Chem.* **1995**, *35*, 691−694.
(28) Li, W.; Klabunde, K. J.; Boronina, T. N.; Zhang, D.; Lagadic, I. *HSRC/WERC Joint Conf. Environ. Albuquerque* **1996**, *16* (Abstr.).
(29) Li, W. F.; Klabunde, K. J. Submitted for publication.
(30) Boronina, T. N.; Klabunde, K. J. 2nd International Conference on Low Temperature Chemistry, Kansas City, 1996; p 171.
(31) Boronina, T. N.; Lagadic, I.; Klabunde, K. J. *HSRC/WERC Joint Conf. Environ. Albuquerque* **1996**, 15 (Abstr.).
(32) Fürstner, A., Ed. *Active Metals. Preparation Characterization, Applications*; VCH Publishers: Weinheim, 1996.
(33) Radzig, V. A.; Bistrikov *Kient. Katal. (Russ.)* **1978**, *XIX*, 713−718.
(34) Hochstrasser, G.; Antonini, J. *Surface Sci.* **1972**, *32*, 644.
(35) (a) Klabunde, K. J. *Free Atoms, Clusters, and Nanoscale Particles*; Academic Press: New York, 1994. (b) Klabunde, K. J.; Cardenas-Trivino, G. in ref *32*, pp 237−275.
(36) Klabunde, K. J.; Ralston, D.; Zoellner, R,; Hattori, H.; Tanaka, Y. *J. Catal.* **1978**, 55, 213.
(37) Cardenas-Trivino, G.; Klabunde, K. J.; Dale, E. B. *Langmuir* **1987**, *3*, 986.
(38) Zuckerman, E. B.; Klabunde, K. J.; Oliver, B. J.; Sorensen, C. M. *Chem. Mater.* **1989**, *1*, 12.
(39) *CRC Handbook of Chemical Physics*, 75th ed.; Lide, D. R., Ed.; CRC: Boca Raton, FL, 1995; pp 12−160.
(40) Solomons, T. W. G. *Organic Chemistry*, 6th ed.; Wiley: New York, 1996; p 413.
(41) Fieser, L. F.; Fieser, M. *Advanced Organic Chemistry*; Reinhold Publishing Co.: London, 1962; p 538.

Received for review November 13, 1997. Revised manuscript received May 4, 1998. Accepted May 22, 1998.

ES970997E